Investigation of the solar wind–Moon interaction onboard Chandrayaan-1 mission with the SARA experiment

Stas Barabash[1,*], Anil Bhardwaj[2], Martin Wieser[1], R. Sridharan[2], Thomas Kurian[3], Subha Varier[3], E. Vijayakumar[3], Veena Abhirami[3], K. V. Raghavendra[3], S. V. Mohankumar[2], M. B. Dhanya[2], Satheesh Thampi[2], Asamura Kazushi[4], Herman Andersson[1], Futaana Yoshifumi[1], Mats Holmström[1], Rickard Lundin[1], Johan Svensson[1], Stefan Karlsson[1], R. Daniele Piazza[5] and Peter Wurz[5]

[1]Swedish Institute of Space Physics, Box 812, 98128 Kiruna, Sweden
[2]Space Physics Laboratory, Vikram Sarabhai Space Center, Thiruvananthapuram 695 022, India
[3]Avionics Entity, Vikram Sarabhai Space Center, Thiruvananthapuram 695 022, India
[4]Institute of Space and Astronautical Science, 3-1-1 Yoshinodai, Sagamihara, Japan
[5]Physikalisches Institut, University of Bern, Sidlerstrasse 5, CH-3012 Bern, Switzerland

The SARA instrument (Sub-keV Atom Reflecting Analyser) comprises a low energy neutral atom (LENA) sensor for the energy range 10 eV–3.3 keV and an ion mass spectrometer (10 eV–15 keV). It is the first ever experiment to study the solar wind–planetary surface interaction via measurements of the sputtered atoms and neutralized back-scattered solar wind hydrogen. The neutral atom sensor uses conversion of the incoming neutrals to positive ions, which are then analysed via surface interaction technique. The ion mass spectrometer is based on the same principle. SARA performs LENA imaging of the Moon's elemental surface composition including that of permanently shadowed areas, and imaging of the lunar surface magnetic anomalies. It will also investigate processes of space weathering and sputtered sources of the exospheric gases.

Keywords: Chandrayaan, elemental composition, energetic neutral atoms, magnetic anomalies, Moon, solar wind.

Introduction

THE Moon does not have an intrinsic magnetic field and atmosphere. The solar wind plasma particles therefore directly hit the Moon's surface. The solar wind (SW) ion energy (around 1 keV protons, 4 keV He^{++}, and several tens of keV multi-charged heavy ions) is high enough and interaction of SW with the lunar regolith results in atomic and ionic sputtering[1], and solar wind particle neutralization and backscattering. The energy of atoms created in these processes exceeds the Moon escape energy (1.62 eV for Fe) and they propagate along straight trajectories similar to photons. Since the energy of the sputtered atoms does not exceed 1 keV, they are called low energy neutral atoms (LENA). By measuring fluxes of these atoms from different directions with a LENA camera, one can build up LENA images and in this way remotely study the solar wind–lunar surface interaction process on the global scale. Since the LENA fluxes depend on the incoming flux of the solar wind particles, simultaneously with LENA measurements one should monitor the solar wind flux.

Science objectives

Imaging the LENA fluxes from the Moon surface addresses the following primary scientific tasks[2,3]: (i) Mapping the elemental composition of the surface including the permanently shadowed areas, (ii) Direct imaging of the surface magnetic anomalies (in sputtered and backscattered LENAs), (iii) Studies of space weathering processes, and (iv) Studies of the sputtered sources of the exospheric gases.

For tightly bound solids the sputtering yield is proportional to the elastic energy transferred by the incident particle to target atoms near the surface. Therefore, the relative yield of different elements reflects the surface composition. The LENA imaging complemented by the solar wind monitoring will thus provide maps of the sputtered yields, which can be converted to coarse surface composition maps. The solar wind particles can reach permanently shadowed areas (e.g. craters in polar regions) due to solar wind thermal spreading, the method thus works even there. Understanding the surface compo-

*For correspondence. (e-mail: stas@irf.se)

sition in these areas is particularly important because the location of the hydrogen-rich areas detected by Lunar Prospector correlates well with the locations of permanent shadow[4]. The hydrogen in these areas is suggested to be in the form of water ice. However, there are speculations that the hydrogen is deposited by the solar wind[5]. Measuring the backscattered hydrogen flux, one can understand the efficiency of solar wind proton deposition in these areas though the direct measurements of the ice sputtering is hardly possible because ice, if any, would be covered by a layer of rigolith/dust.

LENA imaging may also be possible even behind the optical terminator as indicated by the study of Futaana *et al.*[3]. Since the solar wind is a supersonic flow and the Moon is an obstacle to this flow, a void of solar wind is generated behind the Moon. The solar wind flowing behind the obstacle is accelerated by a pressure gradient created by its thermal velocity, enabling its penetration into the void region.

Lunar surface areas with local magnetization with a field magnitude from a few tens of nT to hundreds of nT, and ranging in size from a few km to several hundred km are present over much of the lunar surface[6,7]. The magnetized regions located near the Imbrium and Serenitatis antipodes are 1200 and 700 km wide respectively, with a magnetic field of ~300 nT for the entire region. These anomalies may be strong enough to create 'minimagnetospheres', around 100 km in diameter locally due to interaction with the solar wind[8]. The issue of mini-magnetosphere is still a matter of debate[9]. However, if mini-magnetospheres are created, the solar wind would not be able to reach the surface in these areas and no sputtering of surface material or back scattering will occur. Therefore, the mini-magnetospheres would be visible as decrease in LENA fluxes from these directions[3].

A mini-magnetosphere is still an unproven concept. Its size is close to the proton gyro-radius for the Moon conditions and this effect gives rise to completely new physical phenomena. Two dimensional MHD simulations of the solar wind interaction with the lunar magnetic anomalies[10] have demonstrated that the crustal magnetic fields can hold off the solar wind from the surface and form a 'mini-magnetosphere'. The MHD results also indicated that mini-magnetospheres are much more dynamic than planetary-size magnetospheres. Analysis of observations of non-thermal ions of lunar origin by Particle Spectrum Analyser/Ion Spectrum Analyser onboard Nozomi spacecraft also suggests the formation of mini-magnetospheres[11]. Recent results from the Japanese Kaguya mission also indicate the presence of the mini-magnetospheres[12]. But only LENA imaging provides a direct method to visualize such structure.

Space weathering is a term used to refer to the physical and chemical changes that occur to exposed material on the surface of an airless body as a result of external agents. Apart from micrometeoroid bombardment and electromagnetic radiation, solar wind sputtering is an important contributor to the space weathering on the Moon, and all of them are responsible for the formation and maturation of the lunar regolith as a whole. Space weathering is of considerable interest for studies of surfaces by remote sensing because it causes major changes in the optical properties. It is established in laboratory experiments that the proton irradiation of loose powders results in their darkening and reddening[13]. High albedo at regions of magnetic anomalies is a possible manifestation of this effect[6,14]. Inside the magnetic anomalies, the regolith is shielded from the solar wind flux, because of the formation of a mini-magnetosphere, while the surrounding areas receive a higher flux. Comparison of the maps of the backscattering solar wind hydrogen (normalized to the solar wind conditions) with optical or infrared images can directly reveal the quantitative relations between changes in the albedo and the total dose.

The lunar exosphere is composed of atoms liberated from the lunar surface by meteorite bombardment, photon stimulated desorption (PSD), and sputtering[1]. PSD is the dominant mechanism for Na and K, but only sputtering provides atoms with much higher energies (>10 eV) which thus dominate at higher altitudes. It is established that sputtering contributes significantly to sources of such atoms as Na, K, Al, Mg, Si, Ca[1,15,16]. However, the major problem in quantitative studies of the contribution from sputtering arises from the lack of reliable experimental sputter yields for different species of the mineralogical surface, especially under the prolonged influence of space weathering. All the previous studies rely on laboratory measurements made with specially prepared specimens and theoretical studies dealing with simplified assumptions concerning the structure of the sputtered materials. However, the yields strongly depend on the microstructure of the material (solid, porous, loose aggregates, powders, etc.). It is only the direct measurements in space with real planetary surfaces that can establish these vitally important parameters. Absolute measurements of sputtered LENAs with mass resolution combined with knowledge of the solar wind flux and surface composition will be used to derive the sputter yields. These measurements are of significant importance not only for studies of the lunar exosphere but also for that of Mercury and for asteroids studies.

Instrument configuration

The SARA experiment comprises three units, Chandrayaan Energetic Neutrals Analyser (CENA), Solar WInd Monitor (SWIM) and Digital Processing Unit (DPU) shown in Figure 1. CENA and SWIM interface electrically with the DPU, and the DPU interfaces with the spacecraft. The instrument consumes 17.1 W in total. The SWIM mass is 452 g, CENA 1977 g and DPU 2.0 kg.

Neutrals analyser CENA

CENA is an LENA imaging mass spectrometer. The neutral detection in CENA is based on the conversion of incoming neutrals to ions whose mass is analysed using interaction (reflection and secondary electron release) with a surface. The CENA sensor consists of four subsystems: an ion rejection system, an ionization surface, a photon rejection system, which also performs coarse energy analysis, and a velocity analysis section[17]. The sensor also includes a front-end-electronics (FEE) and a high voltage power supply (HVPS). Figure 2 shows the schematic view of the instrument with typical particle trajectories.

LENAs enter the sensor through an electrostatic-charged particle deflector, which rejects ambient charged particles by a static electric field, as well as collimate the beam. One electrode is grounded and the other one is biased up to +5 kV. The maximum rejection energy is 15 keV. The biased electrode consists of a number of traps to increase particle absorption. The positive polarity does not allow a 'leakage' of secondary electrons. After passing the deflector, the incoming neutrals hit an ionization surface and are converted to positive ions. The ionization surface is a highly polished silicon wafer coated by 300 nm of MgO. The very high smoothness (RMS down to 1 Å) provides high reflection efficiency and high ionization efficiency[18]. The disadvantage of this coating is sensitivity to humidity because MgO is converted to magnesium hydroxide $Mg(OH)_2$ during reaction with water.

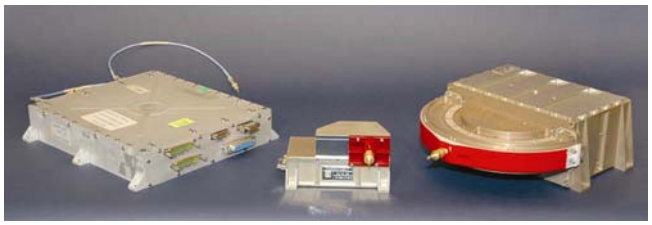

Figure 1. SARA flight model. From left to right are shown the Digital Processing Unit (DPU), the Solar WInd Monitor (SWIM), and the Chandrayaan Energetic Neutrals Analyser (CENA).

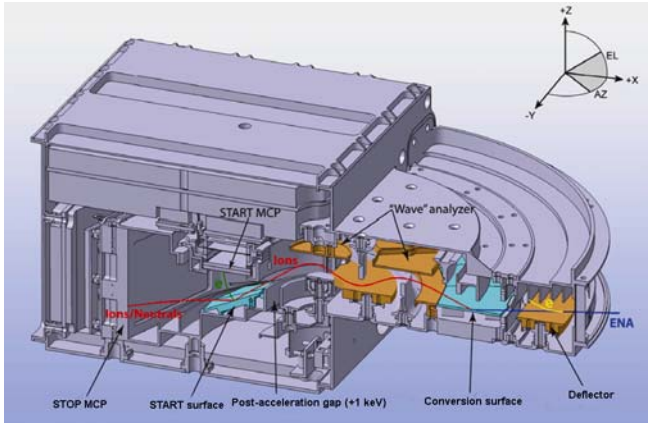

Figure 2. 3D view of the CENA sensor. Typical particle trajectory is also shown.

The neutrals converted to ions pass through an electrostatic analyser of a specific shape (Figure 2). The electric field is such that to pass through the analyser charged particles should move on wave-like trajectories. Photons are not affected by the field, move along straight paths, cannot pass through the wavy-analyser, and are effectively blocked. The 'wave' analyser flat electrodes are serrated and blacked to further increase the photon absorption. The electrostatic 'wave' analyser also provides crude energy analysis. This design is similar to that used in the MTOF sensor of the CELIAS instrument[19] on the SOHO spacecraft, which provides a UV photon rejection factor of 2×10^{-8}. The ions leaving the analyser are post accelerated by a potential of 1.5 kV to reduce spreading in energy caused by the interaction with the conversion surface.

Since the instrument must be capable of measuring masses up to Fe, no carbon foils can be used in the time-of-flight (TOF) section following the analyser. To measure the particle velocity (mass), we use the particle reflection principle developed for and utilized in the Neutral Particle Detector (NPD) of the ASPERA-3 and ASPERA-4 experiments for ESA's Mars and Venus Express missions[20]. After exiting the electrostatic analyser, neutrals converted to ions are post-accelerated, and impact onto a surface, called START surface, at a grazing angle of 15°. During the impact, kinetic secondary electrons are emitted and the particles leaving the surface in different charge states are reflected towards the MCPs where they are detected and produce a STOP pulse for timing electronics. The secondary electrons from the START surface are guided to the START MCPs and produce a START pulse. The START and STOP timing give the particle velocity. Combining the TOF measurements, post-acceleration potential, and the wave analyser settings one determines the incoming LENA energy and mass. Measuring the radius and azimuth of the hit on the START surface by position-sensitive START MCPs allows accurate determination of the TOF length and the arrival azimuth of the incoming particle. The START surface is a polished monocrystalline tungsten. Because of the high atomic number, the surface provides specular reflection with low angular scatter. The secondary electron yield is sufficiently high and the surface properties are stable.

The instrument has seven azimuthal sectors and eight energy steps. The number of the azimuth sectors was chosen in such a way to avoid fringe effects in the central looking direction. The START MCPs are Burle's custom-made plates of a semi-annular shape in the chevron configuration. The START anode uses electron cloud splitting and consists of seven discrete mesh sectors that give azimuth and timing, and four solid ring anodes. STOP MCPs are standard Hamamatsu rectangular plates assembled in the Z-configuration. Four STOP MCPs assemblies

have two discrete solid anodes each and one common grid anode for timing. Four START rings and eight STOP MCPs anodes giving arrival azimuth are used to define the free path length for accurate velocity calculations. Altogether the sensor includes 20 individual preamplifiers (channels), namely, four START rings, seven START azimuth and timing sectors (fast), eight STOP azimuths, and one STOP timing (fast). The signal preprocessing and counting are made by the FEE built around an FPGA (Field Programmable Gate Array) inside the sensor. The FEE also controls HVPS providing seven independently controlled voltages. The main supply generates two (positive/negative) constant +5 kV/–5 kV voltages which are regulated to the required levels by AMPTEK HP601B optocouplers. Table 1 gives the main CENA characteristics.

Solar wind monitor SWIM

SWIM is a very low resource budget sensor optimized for monitoring of the ion fluxes. Figure 3 shows a 3D view of the sensor. The ion flux arrival angle is analysed by an electrostatic deflector consisting of two 90° plates biased to +3.5 kV and to –3.5 kV. Varying voltage applied to the plates sweeps the ion arrival direction over the azimuth from –90° to +90°. The grounded grid in front of deflector screens the deflector electric field and is a part of the ion optics. The electrostatic deflector is followed by a 128° double focusing cylindrical electrostatic analyser. The ions exiting the energy analyser are post-accelerated up to 1 keV by a voltage applied to the TOF cell. The same principle, the particle–surface interaction, to measure the particle velocity as in the CENA is used in the SWIM too. The TOF cell made of graphite to increase UV absorption includes the START and STOP surfaces. The START surface is made of monocrystal polished tungsten. The STOP surface, made of graphite coated by MgO, is optimized for the high secondary electron yield and high UV absorption. The TOF ion optic is optimized to minimize the spot on the START surface and provide a shallow (around 10°) incident angle to increase the secondary ion yield and reflection efficiency. The ions hitting the START surface produce secondary electrons, and are reflected towards the STOP surface. The electrons are collected by a START channel electron multiplier (CCEM) and produce a START pulse. The secondary electrons from the STOP surface are collected by the STOP CCEM and provide a STOP pulse. The timing of the START and STOP events gives the ion velocity and, in combination with known energy, the mass. The energy analyser is equipped with a UV trap inserted into the electrostatic analyser to increase UV absorption of the system. Stepping high voltage on the deflector and analyser provides an azimuth coverage of 180° (the acceptance angle over elevation is 9°) and energy coverage of 10 eV–15 keV. The proposed mass identification approach does not use carbon foils that would require unfeasibly high post-acceleration of heavy ions for such a small sensor. The SWIM FEE is built around two standard AMPTEK A101 hybrid pre-amplifiers, time-to-digital converter GP1, and an controlling FPGA. HVPS is similar to CENA with five individually controlled voltages. Table 1 gives the main SWIM characteristics.

Table 1. CENA and SWIM main characteristics

Parameter	CENA	SWIM
Particle to measure	Neutrals	Ions
Energy range	10 eV–3.2 keV	10 eV–15 keV
Energy resolution	50%	7%
Mass range (amu)	1–56	1–40
Mass resolution	H, O, Na/Mg/Si/Al-group, K/Ca-group, Fe-group	H^+, He^{++}, He^+, O^{++}, O^+, > 20 amu
Full field-of-view	15° × 160°	9° × 180°
Angular resolution	9° × 25° (E > 50 eV)	4.5° × 22.5°
G-factor/sector, w/o	10^{-2} cm^2 sr eV/eV (at 3.3 keV)	1.6×10^{-4} cm^2 sr eV/eV
Efficiency	0.2 cm^2 sr eV/eV (at 25 eV)	
Efficiency (%)	0.01–1	0.1–5
Sensor mass	1977 g	452 g

Digital Processing Unit

The Digital Processing Unit (DPU) provides telemetry (TM), telecommands (TC), and power interfaces for the SARA sensors to the spacecraft (Figure 1). DPU performs

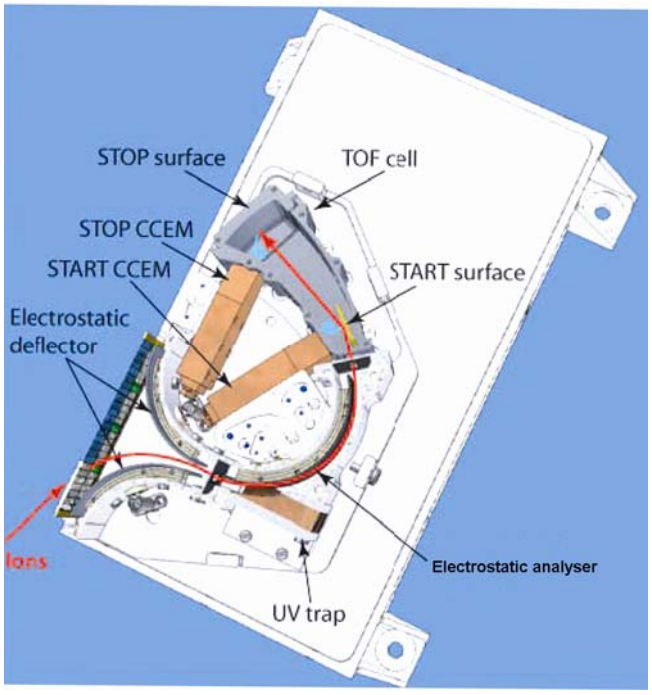

Figure 3. 3D view of the SWIM sensor. Expected ion trajectory is also illustrated.

the sensor control through TCs, sensor data acquisition, processing, compressing to meet telemetry requirements, and transferring packaged data to the satellite TM system. There are independent data and command lines between DPU and the two sensors, interfacing through the LVDS (Low-Voltage Differential Signaling) standard. The data acquisition from the two sensors is simultaneous. Data pre-processing is based on lookup tables and mathematical computations. The processed data are subjected to lin-log compression followed by the RICE loss-less compression and transferred to the spacecraft TM system. TC are used for sensor power on/off, direct commanding, altering the processing parameters as well as for updating the onboard memory contents.

The DPU is built around ADSP21060 DSP processor running at 32 MHz clock frequency and having 4 Mbit on-chip memory for operational software. CENA interface, TM interface and power control are built into ACTEL FPGA RT1280. Look-up tables for the command related parameters and parameters for data processing are stored in 1 Mbit EEPROM (Electrically Erasable Programmable Read-Only Memory). Two 16 Mbit SRAM (Static Random Access Memory) are used for storing the processed data and a 128 Kbit DPRAM (Dual-Ported Random Access Memory) is used for TM buffering. The DPU has the capability for patching (reprogramming) the onboard software residing in the internal memory of the processor. There is a built-in provision to modify the EEPROM contents at any time in orbit and read back for correctness. Macro commanding feature is designed in the system for execution of commands pre-stored in DPU. Also, the software is designed in such a way that the total operation of the sensors can be directly controlled from ground by TCs. Watch dog reset function is implemented for resetting the system in case of an upset in software scheduling.

Science data are transferred to the spacecraft's Data Handling Unit (DHU), house keeping (HK) data both fast (one package per 2 s) and slow (one package per 32 s) to the spacecraft Bus Management Unit (BMU). The data transfer, TC reception, data ready polling and OBT (On Board Timer) time acquisition are carried out through a MIL-STD-1553 bus. The total allotted bandwidth of SARA is apportioned between CENA and SWIM in real time, depending on the data availability from the two sensors for full utilization of the available bandwidth. The peak data transfer rate from DPU to the spacecraft is 28 kbps and the average data rate is 4 kbps over 12 h. There is no fixed scheduling for the data transfers. Data are transferred on request only, which is handled by the processor, depending on the processed data availability from the sensors. The operational and TM sensor modes are set by DPU through TCs. In the non-process mode the raw data received from the sensors are sent to DHU as such. The system can operate in various configurations, with only one or two sensors ON, with multiple integration cycles for processing, with compression enabled or disabled, one sensor in processing mode and the other sensor in the non-process mode.

The DPU power board converts the primary bus voltage (+28 V to +42 V) to the regulated secondary voltages (±12 V, +3.3 V, +5 V) for powering the DPU processing electronics and sensors. DPU is switched on by a relay command from the spacecraft but the sensors are totally under the DPU control. Sensor power on/off and power sequencing requirements are built into the DPU power board. There is also a provision in BMU for switching sensors off directly in case of a 1553 bus failure.

Calibrations

Calibrations of both sensors were performed at the Swedish Institute of Space Physics, Kiruna, with ion beam calibration facility. The ion beam source provides large diameter (up to 10 cm) beams of different masses in the energy range 100 eV to 50 keV. The facility is equipped with 4 degree of freedom turn table, and data and house keeping parameter acquisition system. The beam intensity is measured by either a Faraday cup or a grid anode inserted into the beam (continuous monitoring). The facility provides vacuum down to few 10^{-7} mbar.

CENA was calibrated using both ions (H^+, H_2O^+, N^+, N_2^+, Ar^+) and respective neutrals produced in the original beam via charge-exchange on the residual gas. The neutral component is about 0.1–1% of the original beam intensity depending on the vacuum conditions. The neutral beam intensity cannot be monitored, and the neutral beams were used only to verify performance of the entrance ion optics. The characteristics determined in the CENA calibrations are pixel's sensitivity and angular response for difference masses and energies, times of flight for different masses and energies to be used in onboard look-up table for mass identification, and deflector efficiency (only checks). Figure 4 shows TOF spectra recorded by CENA exposed to 1.3 keV beams of different ions. The N^+ (14 amu, O-group) and H_2O^+ (18 amu, Na/Mg/Si/Al-group), and Ar^+ (44 amu, K/Ca-group) are resolved. The secondary peaks (20–50% intensities) at faster times of flight visible for species heavier than 3 amu result from recoil process. A heavier particle hitting the START surface transfer momentum to lighter species mostly hydrogen in water layer, which may have been deposited on the surface.

SWIM was calibrated in similar manner as the CENA using the same ion species. The characteristics determined in the SWIM calibrations are sensor sensitivity, pixel's angular response for different masses and energies to calculate geometrical factor, times of flight for different masses and energies to be used in onboard look-up table for mass identification, analyser and deflector constants. Both SWIM and CENA performances were found to be close to those presented in Table 1.

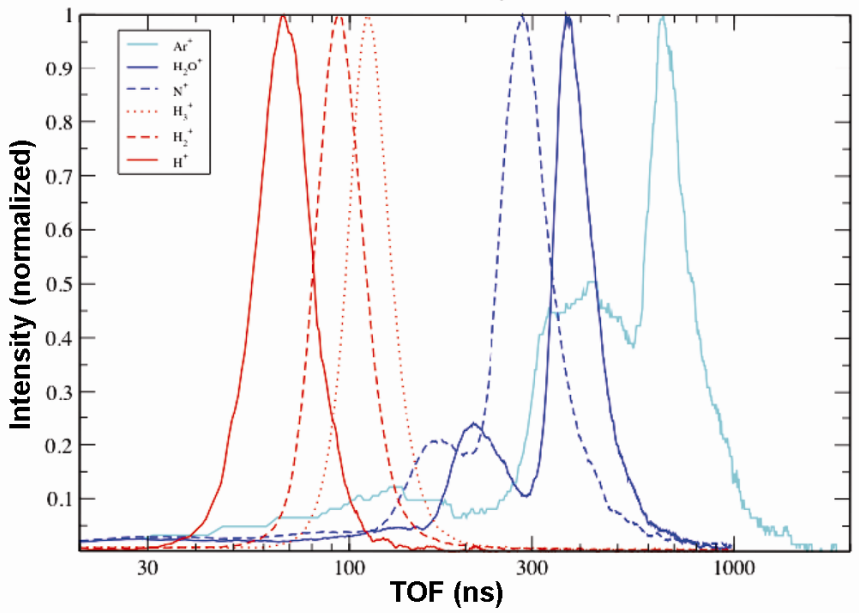

Figure 4. CENA time-of-flight spectra for 1.3 keV beams of different mass ions. The deflector is off.

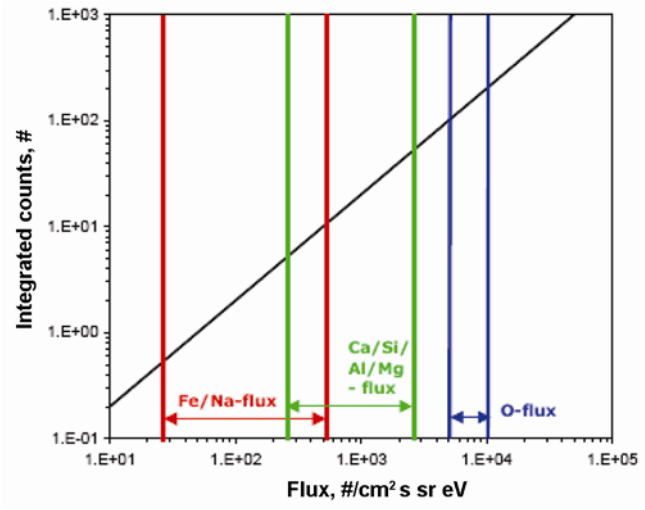

Figure 5. The expected flux ranges for different sputtered products[3] and the CENA response (integrated counts/8 s).

Expected results and challenges

The most exciting results will probably concern imaging of the lunar magnetic anomalies. Does the solar wind really stop and cannot reach the surface as was proposed[8] by the Lunar Prospector team? If it does, what would be the shape of the void? Physics of the Moon's mini-magnetospheres is completely unknown and challenging because the mini-magnetospheres, if created, fall into the intermediate scale range. The typical size (~100 km) is close to the proton gyroradius (30–150 km) but larger than electron gyroradius. A detail study of the issue suggests that the CENA-type of instrument can readily identify solar wind voids of a size of 50 km (CENA on ground resolution for the central pixel) as drops in sputtered ion flux[3]. In the light of the latest Kaguya results[12] indicating the high resolution efficiency of the Moon rigolith (the flux of reflected hydrogen will be much higher than the measured 1% reflection efficiency for protons), the hydrogen flux from the neutralized solar wind provides better means to image solar wind voids because of much higher intensity.

CENA will make the first ever attempt to detect sputtered atoms from the lunar surface. The fluxes of sputtered atoms for typical solar wind conditions have been estimated[3]. Figure 5 shows the flux ranges for different species and the CENA response (accumulated counts). We use the CENA geometrical factor (Table 1), efficiency 0.1% and the accumulation time 8 s, which is close to the time, a point object on the Moon surface is within CENA field of view while the spacecraft moves on a 100 km orbit. Oxygen fluxes will result in more than 100 counts, the group of atoms with atomic masses from 24 to 40 amu (Mg, Al, Si, Ca) in around 10 counts, and Fe and Na in a few counts. CENA will scan the Moon surface and maps of the neutral atom emissions will be constructed. These maps will be compared with topographical, albedo mineralogical maps, and calibrated against elemental maps. That would allow us to understand how different minerals and lunar areas interact with the solar wind. Of particular interest is to investigate the composition of the sputtered neutral flux from the permanently shadow areas which are nevertheless reachable by the solar wind plasma due to thermal spreading. Will the composition differ significant from the nearby areas?

Replicas of the CENA and SWIM sensors will fly to Mercury onboard BepiColombo, a joint mission between

European Space Agency and Japan Aerospace Exploration Agency, with launch scheduled for 2013 (refs 21, 22). Mercury resembles the Moon in terms of plasma–surface interaction, and Chandrayaan-1 and BepiColombo present a unique opportunity for comparative studies of these two atmosphere-less bodies.

1. Wurz, P., Rohner, U., Whitby, J. A., Kolb, C., Lammer, H., Dobnikar, P. and Martín-Fernández, J. A., The lunar exosphere: the sputtering contribution. *Icarus*, 2007, **191**, 486–496.
2. Bhardwaj, A. *et al.*, Low energy neutral atom imaging on the Moon with the SARA Instrument aboard Chandrayaan-1 mission. *J. Earth Sys. Sci.*, 2005, **114**, 749–760.
3. Futaana, Y., Barabash, S., Holmström, M. and Bhardwaj, A., Low energy neutral atoms imaging of the Moon. *Planet Space Sci*., 2006, **54**, 132–143.
4. Feldman, W. C. *et al.*, Evidence for water ice near the lunar poles. *J. Geophys. Res.*, 2001, **106**, 23231–23252.
5. Feldman, W. C., Lawrence, D. J., Elphic, R. C., Barraclough, B. L., Maurice, S., Genetay, I. and Binder, A. B., Polar hydrogen deposits on the Moon. *J. Geophys. Res*., 2000, **105**, 4175–4195.
6. Hood, L. L., Zakharian, A., Halekas, J., Mitchell, D. L., Lin, R. P., Acuna, M. H. and Binder, A. B., Initial mapping and interpretation of lunar crustal magnetic fields using Lunar Prospector magnetometer data. *J. Geophys. Res*., 2001, **106**, 27825–27839.
7. Halekas, J. S., Mitchell, D. L., Lin, R. P., Frey, S., Hood, L., Acuna, M. and Binder, A. B., Mapping of lunar crustal magnetic fields using Lunar Prospector electron reflectometer data. *J. Geophys. Res*., 2001, **106**, 27841–27852.
8. Lin, R. P. *et al.*, Lunar surface magnetic fields and their interaction with the solar wind: Results from Lunar Prospector. *Science*, 1998, **281**, 1480–1484.
9. Halekas, J. S., Delory, G. T., Brian, D. A., Lin, R. P. and Mitchell, D. L., Density cavity observed over a strong lunar crustal magnetic anomaly in the solar wind: A mini-magnetosphere? *Planet. Space Sci*., 2008, **56**, 941–946.
10. Harnett, E. M. and Winglee, R. M., 2.5-D particle and MHD simulations of mini-magnetospheres at the Moon. *J. Geophys. Res.*, 2002, **107**, 1421, doi:10.1029/2002JA009241.
11. Futaana, Y., Machida, S., Saito, Y., Matsuoka, A. and Hayakawa, H., Moon-related nonthermal ions observed by Nozomi: Species, sources, and generation mechanisms. *J. Geophys. Res.*, 2003, **108**, 1025, doi:10.1029/2002JA009366.
12. Saito, Y. *et al.*, Solar wind proton reflection at the lunar surface: Low energy ion measurements by MAP-PACE on board SELENE (KAGUYA). *Geophys. Res. Lett.*, 2008, **35**, L24205. doi: 10.1029/2008GL036077.
13. Hapke, G., Space weathering from Mercury to the asteroid belt. *J. Geophys. Res*., 2001, **106**, 10039–10073.
14. Richmond, N. C., Hood, L. L., Halekas, J. S., Mitchell, D. L., Lin, R. P., Acuna, M. and Binder, A. B., Correlation of a strong lunar magnetic anomaly with a high-albedo region of the Descartes mountains. *Geophys. Res. Lett.*, 2003, **30**, 1395, doi: 10.1029/2003GL016938.
15. Potter, A. E. and Morgan, T. H., Variation of lunar sodium emission intensity with phase angle. *Geophys. Res. Lett*., 1994, **21**, 2263–2266.
16. Killen, R. M. and Ip, W.-H., The surface-bounded atmospheres of Mercury and the Moon. *Rev. Geophys*., 1999, **37**, 361–406.
17. Kazama, Y. *et al.*, Energetic neutral atom imaging mass spectroscopy of the Moon and Mercury environments. *Adv. Space Res.*, 2006, **37**, 38–44.
18. Wieser, M., Wurz, P., Brüning, K. and Heiland, W., Scattering of atoms and molecules off a magnesium oxide surface. *Nucl. Instr. Meth. B*, 2002, **192**, 370–380.
19. Hovestadt, D. *et al*., CELIAS – Charge, Element and Isotope Analysis System for SOHO. *Solar Phys*., 1995, **162**, 441–481.
20. Barabash, S. *et al*., The Analyzer of Space Plasmas and Energetic Atoms (ASPERA-3) for the Mars Express mission. *Space Sci. Rev*., 2006, **126**, 113–164.
21. Schulz, R., BepiColombo payload and mission updates. *Adv. Space Res*., 2006, **38**, 572–577.
22. Van Casteren, J., Novara, M., Best, R., Hayakawa, H. and Ferri, P., The BepiColombo Mission. *Planet. Space Sci.*, 2008, in press.

ACKNOWLEDGEMENTS. The efforts at the Swedish Institute of Space Physics and University of Bern were supported in part by European Space Agency.